PCCP

Accepted Manuscript

ROYAL SOCIETY OF CHEMISTRY

www.rsc.org/pccp

Journal Name

RSCPublishing

ARTICLE

Computational and Ion Mobility MS Study of *(all-S)*-cyclohexylhemicucurbit[6]uril Structure and Complexes

Cite this: DOI: 10.1039/xoxxoooooox

Received ooth January 2012,
Accepted ooth January 2012

DOI: 10.1039/xoxxoooooox

www.rsc.org/

Mario Öeren, Elena Shmatova, Toomas Tamm and Riina Aav*

A computational study of (*all-S*)-cyclohexylhemicucurbit[6]uril and its complexes with anions (Cl^-, Br^-, I^- and $HCOO^-$), the proton (H^+) and non-dissociated acid (HCl, HBr, HI and HCOOH) guests was performed. The geometries of guest-host complexes were optimized via density functional theory using BP86 functional, SV(P) basis set and Stuttgart pseudopotentials for iodide. Binding affinities and their trends were evaluated at the BP86/TZVPD level of theory. In addition, the Quantum Theory of Atoms In Molecules was used to gain insight into guest-host interactions. A computational study in a gas phase and ion-mobility mass-spectrometry analysis revealed that the studied macrocycle formed inclusion complexes with anions. Protonation of the macrocycle is preferred at the nitrogen atom pointing inside of the cavity. In the studied conditions, non-dissociated acids formed complexes at the oxygen atom pointing outside of the macrocycle.

1. Introduction

Although the first cucurbituril (CB) was synthesized more than 100 years ago,[1] and characterized over 30 years ago,[2] this macrocyclic compound has gained wider attention only in recent decades. Applications of CBs[3] are based on their ability to bind guest molecules, mainly alkylammonium cations. CBs are widely used as catalysts,[4] nanomaterials and as drug delivery vehicles[5]. Hemicucurbiturils (HCs) are a relatively new branch in the diverse CB family.[3] The first HCs (HC[*n*] with n = 6, 12) were synthesized by Miyahara *et al.*[6] in 2004 and since then only a few new HCs have been reported[7–9] . Amongst new HCs, the first enantiomerically pure member of the cucurbituril family, (*all-S*)- and (*all-R*)-cyclohexylhemicucurbit[6]uril (cycHC[6]), has been synthesized in our group.[10] Unsubstituted HCs have been reported to catalyse organic reactions[11–13], although their mode of action is still unknown. Contrary to CBs, in which the urea units are aligned, HCs adopt a 'zig-zag' orientation, causing a substantial difference in the electronic structure of the macrocycle and thereby allowing for the binding of anions.[6,14] The anion binding properties of structurally close relatives of hemicucurbiturils, namely bambus[*n*]urils[15] (BU[*n*], n = 4 - 6) have also been reported.[16–18]

Since the pioneering computational study of Kim and co-workers in 2001,[19] there has been a steady increase in the number and quality of computational treatments of cucubiturils and related systems. In many cases, complexation with various guest molecules has been among the goals of the studies. The size of the system, which is further increased by inclusion of a guest, initially necessitated the use of relatively simple models (Hartree-Fock) and small basis sets (STO-3G, 3-21G)[19–21]. Recent advances in computer technology have made treatments with more sophisticated models (DFT with hybrid functionals, up to triple-zeta basis sets) feasible[22–32]. Use of the density fitting (also known as Resolution of Identity) approximation is routinely used, especially because the associated loss in accuracy is negligible.

Several researchers have paid close attention to the frontier molecular orbitals – the highest occupied MO (HOMO) and lowest unoccupied MO (LUMO) – of the macrocyclic systems[24,25,33], as well as the electrostatic potential generated by the molecule[26–32]. These properties lead to the prediction of binding sites and modes of guests, and HOMO-LUMO energy gaps can be used as indicators of relative reactivities. The map of electrostatic potential (MESP) outlines electron-rich and electron-poor regions of a macrocycle, which are indicators of locations of possible electrostatic interactions between the host and the guest.

Binding modes and binding energies of various guest molecules have also received research attention[19,21,25,34–36]. Such models can also provide insight into the probable location of the binding site, including whether binding inside or outside of the macrocycle is preferred. Additional information about the nature of chemical bonds between the host and guests has been obtained from the quantum theory of atoms in molecules (QTAIM)[23,31]. This model also provides an estimate of the strength of host-guest interactions.

It has been reported that the HC binds anions[9,23,37] and a few cations[38,39]. In addition, Cong *et al*. have suggested that the binding of a proton inside of HC occurs during catalysis with HC.[12] The chiral hemicucuribituril (*all-S*)-cycHC[6] was isolated as a hydrogen halide complex. Aditionally, based on the results of a diffusion NMR study of (*all-S*)-cycHC[6] complexes, it was proposed that substituted hemicucurbituril forms inclusion complexes with carboxylic acids[10]. So far, there is no crystal structure of (*all-S*)-cycHC[6] complexes and it is not known whether the acids are bound as dissociated anions or as non-dissociated neutral species. A computational study of the structure and mode of complexation of cycHC[6] would increase our knowledge in this field.

In this paper, we report the geometry and electronic structure of cycHC[6] and its complexes with the anions Cl^-, Br^-, I^- and HCOO and the proton and non-dissociated (HCl, HBr, HI and HCOOH) guests. Different binding sites were evaluated and selected complexes were studied using QTAIM analysis. Additionally, a study of ion mobility mass-spectrometric analysis of cycHC[6] complexes was performed.

2. Experimental Section

2.1 Computational Details

2.1.1 Description of the opening and the cavity of cycHC[6]. Four parameters were chosen to describe the geometric changes of the macrocycle upon complexation with guests. The distances from the carbon C_2 and oxygen O to the centre of the cavity X ($r(C_2\text{-X})$ and $r(\text{O-X})$) describe the changes of the geometry at the equator of the macrocycle. The distances from the C_{4a} and C_7 to the centre of the cavity ($r(C_{4a}\text{-X})$ and $r(C_7\text{-X})$) describe the opening or closing movement of the cyclohexyl groups. The shortest distance of C_5 from the axis (Z) ($r(C_5\text{-Z})$) describes the openings of the macrocycle. The listed distances are graphically depicted in Figure 1. The cavity size of the optimized structures was studied with the program Swiss-PdbViewer.[40]

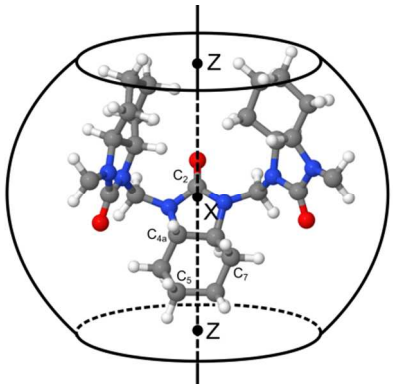

Fig.1. Atom numbers, centre of the cavity and axis of cycHC[6].

2.1.2 Electronic structure calculations. All molecular structures in this work were built with the program Avogadro[41] and pre-optimized therein using the MMFF94 molecular-mechanical model. Further geometry optimizations were conducted with density functional theory (DFT), using the BP86 functional[42–46] along with the def2-SV(P)[47] basis set. The interactions between guest and host were expected to be prevailingly electrostatic; hence, in the interest of computational speed, the choice of the lightweight, thus fast functional without dispersion correction was justified. To speed up the geometry optimization, the resolution of identity (RI) approximation was used.[48–51] Vibrational frequency calculations were performed to ensure that all chosen geometries were at minima, and to estimate the zero-point vibrational energies (ZPE). The energies of local minima were refined by single-point calculations with the def2-TZVPD[47] basis set. The iodine atoms were described with inclusion of the appropriate Stuttgart pseudopotential[52,53]. In addition, counterpoise correction calculations were performed to obtain basis set superposition error (BSSE) corrected energies for host-guest complexes.[54] The transition states were verified using dynamic reaction coordinate calculations. All calculations were performed in the gas phase. Solvation effects were omitted because cycHC[6] complexation was previously studied in hydrophobic solvent ($CDCl_3$)[10] and to model that one should include the first shell explicitly and use a continuum model to describe the bulk solvent. Currently, little information is available about the structure of the first explicit solvation shell of chloroform for the calculated species. Also, in this work complexes were experimentally studied in the gas phase by mass-spectrometric analysis. The Density Functional Theory calculations were performed using the Turbomole 6.4 program package.[55–58]

2.1.3 Search for binding sites. The search for binding sites for guests was done systematically, where outside of the macrocycle five latitudes (with 36° increments) and five longitudes (with 10° increments) were combined (Figure 2).

The crossing points of the meridians and parallels were used as initial locations for the guests in the geometry optimizations. For each guest type, a few locations were added manually as well. The centre of the macrocycle was added to the set for anions and locations on the HOMO were added for the proton. The combinations of anion and proton locations were added for the non-dissociated guest.

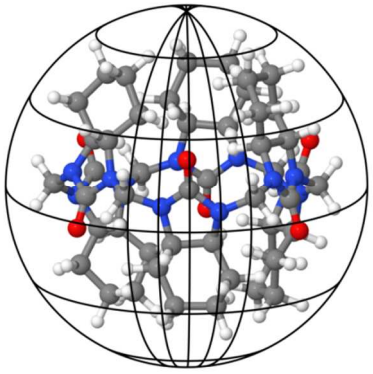

Fig.2. Latitudes and longitudes used in a systematic search for binding sites.

2.1.4 Binding energy of the guest. The binding energy (BE) was calculated by subtracting the sum of the total energies of the reagents from the sum of the total energies of the products. The total energies for each geometry were calculated as sums of DFT energies (DE) and basis set superposition error (BSSE) corrections from def2-TZVPD calculations and the zero-point energy (ZPE) correction from def2-SV(P) calculations. The binding energy of anions and non-dissociated guests with the host were calculated according to equation 1.

$$BE = (DE_{GH} + ZPE_{GH} + BSSE_{GH}) - (DE_G + ZPE_G + DE_H + ZPE_H)\,, \quad (1)$$

where the equation components with the subscripts GH, G and H denote the aforementioned energies of the guest-host complex, guest and host, respectively.

The calculation of the binding energy of a proton to the macrocycle is shown in equation 2, and it was found via the reaction of an oxonium ion with a host molecule, producing water as the second product.

$$BE = (DE_{GH} + ZE_{GH} + DE_{H2O} + ZE_{H2O}) - (DE_{H3O+} + ZE_{H3O+} + DE_H + ZE_H)\,, \quad (2)$$

where the equation components with the subscripts GH, H_2O, H_3O^+ and H denote the aforementioned energies of the guest-host complex, water, oxonium ion and host, respectively.

2.1.5 Post-processing of the results. For visualization of the map of electrostatic potential (MESP), single-point calculations were repeated at the def2-SV(P) level of theory using Gaussian 09[59] software. Visualizations of geometries, frontier orbitals and MESP were generated from the output files with Jmol[60] and Molekel[61]. The binding properties of the macrocycle were studied via QTAIM,[62] using the program Multiwfn[63] with def2-SV(P) density. The required .wfx file for iodine with ECP information was generated with Gaussian 09. Interactions between the host and the guest were investigated via locating the bond critical points (BCPs) as defined in the QTAIM model. The interaction energies (E) were calculated using the potential energy density (V) at the corresponding BCP, as in this case E = V/2.[64]

2.2 Ion-mobility mass-spectrometric analysis

Hemicucurbituril cycHC[6] HCl and HBr adducts were synthesized as previously described.[10] 40μM solutions of cycHC[6] + HCl and cycHC[6] + HBr in a solvent mixture of H_2O (47.5%), MeOH (47.5%) and HCOOH (5%) were prepared and analyzed by electrospray ionization ion mobility mass spectrometry (ESI-IM-MS). All of the MS experiments were performed using a Waters Synapt G2 HDMS quadrupole travelling wave ion mobility orthogonal acceleration time-of-flight mass spectrometer (Waters, Manchester, U.K.), equipped with a normal Z-spray ESI source in both positive and negative ion modes. A source temperature of 100 °C, capillary voltage of 2 kV, desolvation temperature of 150 °C, and cone voltage of 20 V were set as the ESI parameters. All experiments were performed in conditions with 280 m/s of wave velocity and 18 V of wave height by traveling wave ion-mobility mass spectrometry (TWIM-MS). The experimental collision cross sections (Ω_D) of cycHC[6] complexes were calculated by the calibration method of Thalassinos *et al*,[65] with polyalanine as a calibrant. The published Ω_D values of the polyalanine were obtained from the database of the Clemmer group[66]. The theoretical Ω_D values were calculated by the projection approximation method, using the radius of each atom[67] from the hard sphere mode[68].

3. Results and discussion

3.1 Geometry and electronic structure of cyclohexylhemicucurbit[6]uril.

The calculated structure of cycHC[6] had monomers in 'zig-zag' orientation and exhibited D_3 point group symmetry. Validation of the computed structure was done via comparison of the shortest distances between the centre of the cavity, axis and selected atoms - $r(C_5\text{-Z})$, $r(C_7\text{-X})$, $r(C_{4a}\text{-X})$, $r(C_2\text{-X})$ and r(O-X) - of the calculated and crystallographic structure[10] (Table 1).

Table 1. Distances between the centre of the cavity and axis and selected atoms of computed and experimental cycHC[6] in Å.

	Computed parameters	Experimental parameters[a]
$r(C_5\text{-Z})$	3.1	2.7 ± 0.2
$r(C_7\text{-X})$	4.2	3.8 ± 0.1
$r(C_{4a}\text{-X})$	4.2	4.1 ± 0.1
$r(C_2\text{-X})$	4.4	4.4 ± 0.2
r(O-X)	5.0	5.0 ± 0.1

[a] radii were the mean values for six atoms of each monomer given with maximum absolute deviation.

As can be seen from Table 1, the distances $r(C_2\text{-X})$ and r(O-X) of the computed structure were very close to the experimental ones, while the difference increased for the atoms that were located closer to the opening from $r(C_{4a}\text{-X})$ to $r(C_5\text{-Z})$. The differences between the computed and experimental structure were probably caused by the flexibility of cyclohexyl groups, which were influenced by the packing forces in the crystal structure. The volume of the internal cavity was 22 Å^3 for the calculated structure and 18 Å^3 for the experimental structure.

The highest occupied molecular orbital (HOMO) was mostly distributed over the polar cyclic urea functional groups, and its bulkiest lobes were on the nitrogen atoms (Figure 3, a). Nitrogen atoms were not planar, adopting quasi-sp^2/quasi-sp^3 geometry, therefore the HOMO lobes on nitrogen atoms were present both inside and outside of the macrocycle. The HOMO was located also on cyclohexyl moiety and this orbital only

slightly covered the oxygen atoms. The location of the binding site for cations was not uniquely determined by the orbital structure. The binding of a cation could take place inside or outside of the macrocycle, where the HOMO of the latter was delocalized. The lowest unoccupied molecular orbital (LUMO), on the other hand, was concentrated mostly inside the macrocycle (Figure 3, b).

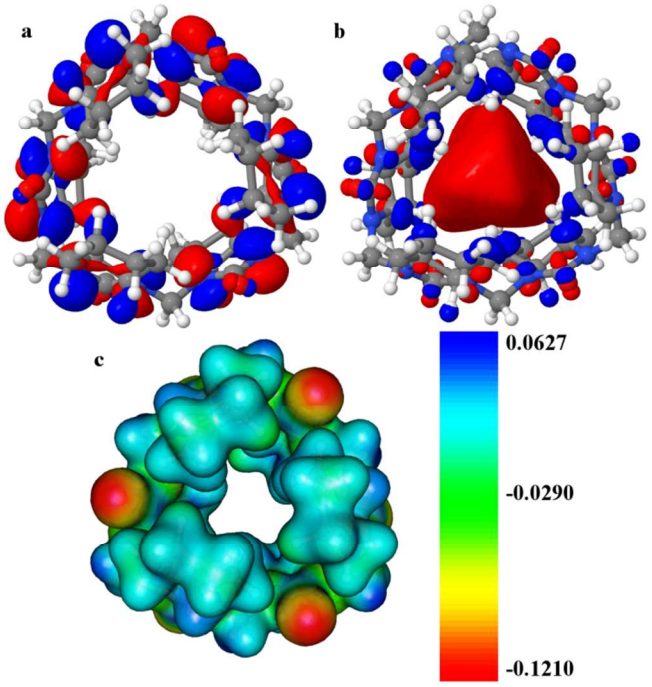

Fig.3. Electronic structure of cycHC[6]: a) HOMO; b) LUMO; c) MESP

This positioning of the LUMO in the centre of the cavity creates a potential binding site for anions. Therefore, we could expect interaction between the HOMO of the anionic guests and the LUMO of macrocycle, which would result in encapsulation of the anionic guest molecule. The HOMO-LUMO gap was 4.93 eV (SV(P)), making it the lowest amongst analogous macrocycles (6.04 – 6.58 eV)[23].

The map of electrostatic potential (MESP) of cycHC[6] is shown in Figure 3, c. The most electron-rich regions (red area) were on oxygen atoms, while the most electron-deficient areas (blue areas) were found on the methylene bridges and the centres of cyclohexyl groups. Besides oxygen atoms, nitrogen atoms were found to be electron-rich as well (yellow area) and, due to the chirality of the monomer, one electron-rich nitrogen was pointing outside of the macrocycle and the other one inside. The MESP on nitrogen atoms agreed with the HOMO being located on the nitrogen atoms. The openings of the macrocycle were rather electron-poor. The listed characteristics of cycHC[6] electronic structure and frontier orbitals made it possible to visualize possible binding sites of guest molecules. However the complexation of both an anion and a proton inside the cavity of macrocycle are feasible. Further computations of the interaction strengths and binding energies of non-dissociated and dissociated acids with cycHC[6] were carried out.

3.2 Structure of cycHC[6]–anion complexes.

In the search for the binding sites for anions, geometry optimization of all generated initial structures led to multiple distinct local minima for all anions. In all cases, anions strongly preferred the binding site inside the macrocycle. The energy difference between the lowest-energy minimum, having an anion inside, and the second-lowest one, having an anion outside, was always over 25 kJ/mol and reached 100 kJ/mol for some higher-lying minima. Based on these results, we propose that all anions prefer to reside inside the macrocycle. The lowest energy complexes are shown in Figure 4. All possible molecular geometries of different binding sites and their energies can be found in the supporting information.

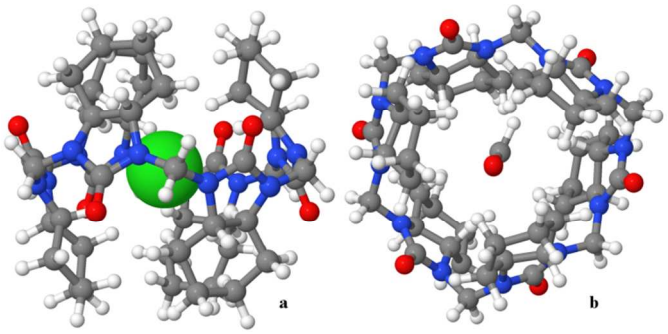

Fig.4. Lowest energy complexes of cycHC[6] with anions Cl^- (a) and $HCOO^-$ (b).

The shortest distances between inside-pointing axial hydrogens ($H5_{ax}$, $H7_{ax}$, $H4a_{ax}$), carbonyl carbon (C_2) and the centre of the cavity (X) and axis (Z) were measured to compare the geometries of anion complexed macrocycles and non-complexed macrocycles. The relevant distances $r(H5_{ax}\text{-}Z)$, $r(H7_{ax}\text{-}X)$, $r(H4a_{ax}\text{-}X)$ and $r(C_2\text{-}X)$ are given in Table 2.

Table 2. Distances between the centre of the cavity, axis and selected atoms of non-complexed and complexed cycHC[6] with anions in Å. Cavity volumes are given without a guests in $Å^3$.

	Non-complexed cycHC[6]	cycHC[6] complexed with			
		Cl^-	Br^-	I^-	$HCOO^-$
$r(H5_{ax}\text{-}Z)$	2.4	2.2	2.3	2.4	2.3 – 2.4[a]
$r(H7_{ax}\text{-}X)$	3.2	3.0	3.1	3.2	3.0 – 3.1
$r(H4a_{ax}\text{-}X)$	3.2	3.0	3.0	3.1	3.0 – 3.2
$r(C_2\text{-}X)$	4.4	4.5	4.5	4.5	4.4 – 4.5
Cavity volume	22	21	21	22	21

[a] Minimum and maximum distances are given due to the asymmetrical geometry of the complexes with this anion.

All spherical halogen anions caused symmetrical changes in the geometry of cycHC[6], while the non-spherical formic acid anion led to deformation of the macrocycle. Upon adopting the anions inside the cavity of the macrocycle, the distance $r(C_2\text{-}X)$ increased, showing that the equator of the cycHC[6] had expanded slightly. At the same time, the distances between the inside-pointing hydrogens of the cyclohexyl rings and axis, as

well as the centre of the cavity (r($H5_{ax}$-Z), r($H7_{ax}$-X), r($H4a_{ax}$-X)) decreased, indicating that flexible cyclohexyl rings covered the anions, causing a slight shrinkage of the opening. The biggest changes in cavity size took place in the case of chloride and the smallest with iodine complex.

According to QTAIM analysis, halogen anions had 12 bonding interactions with the macrocycle. All halogen anions interacted with the same hydrogens ($H4a_{ax}$ and $H7_{ax}$) of each monomer of the macrocycle. The calculated interaction energies were close to 5 kJ/mol for both interacting hydrogens and similar for each halogen anion. The $HCOO^-$ ion interacted with the same hydrogen atoms, although the interaction energies showed large variability (3.0 – 14 kJ/mol). Additionally, the $HCOO^-$ formed two extra bonding interactions between the formate hydrogen atom and two nitrogen atoms of different monomers of the macrocycle (H-N interactions (*a*) and (*b*) in Table 3).

The binding energies of the four anions with the host molecule were computed according to the reaction of cycHC[6] with anion X^-, as shown below. The binding and interaction energies of anion complexes are listed in Table 3.

$$X^- + \text{cycHC[6]} \rightarrow X^-@\text{cycHC[6]}$$

Table 3. Interaction and binding energies (kJ/mol) of anions with cycHC[6].

	Cl^-	Br^-	I^-	$HCOO^-$
Average interaction energies	4.7	4.9	4.8	9.7[a]
H-N (*a*)	-	-	-	7.3
H-N (*b*)	-	-	-	4.5
Sum of interaction energies	56.7	59.1	58.0	127.8
Binding energy	-99	-87	-65	-83

[a] The average interaction energy for $HCOO^-$ does not contain H-N energies.

Despite the fact that formate had the highest interaction energy with cycHC[6] (127.8 kJ/mol), the binding energy showed the strongest interaction with chloride (-102 kJ/mol), in the gas phase, as chloride fit best into the macrocycle. Distortion of the macrocycle geometry by the $HCOO^-$ ion partially cancelled the effect of the strong interactions by increasing tension in the macrocycle. In the case of halides, the interaction energies decreased with the increase in the size of the halide, which could have been caused by the repulsive force between the anion and heavy atoms of the macrocycle. These computational results agree well with the LUMO localization inside of the non-complexed macrocycle and confirm that cycHC[6] forms inclusion complexes with halogen and formate anions.

In addition to binding energy, the transition states of ion insertion were studied as well. While Cl^- and Br^- insertion is spontaneous, the transition state energies for I^- and $HCOO^-$ insertion are 22 kJ/mol and 12 kJ/mol respectively. (Figure 5) At the start of the ion insertion both anions were bound at the opening of the macrocycle. Energies of the corresponding local minima at the opening were higher than the global minima by 11 kJ/mol for I^- and 20 kJ/mol for $HCOO^-$, respectively. During the transition, anions moved along the Z axis, the cyclohexyl groups opened up: the *r*($H5_{ax}$-Z) increased from the value of 2.4 Å up to 3.6 Å. This indicates that the studied anions have low or no insertion barriers which means that the formation of the inclusion complexes is favored.

Journal Name RSCPublishing

ARTICLE

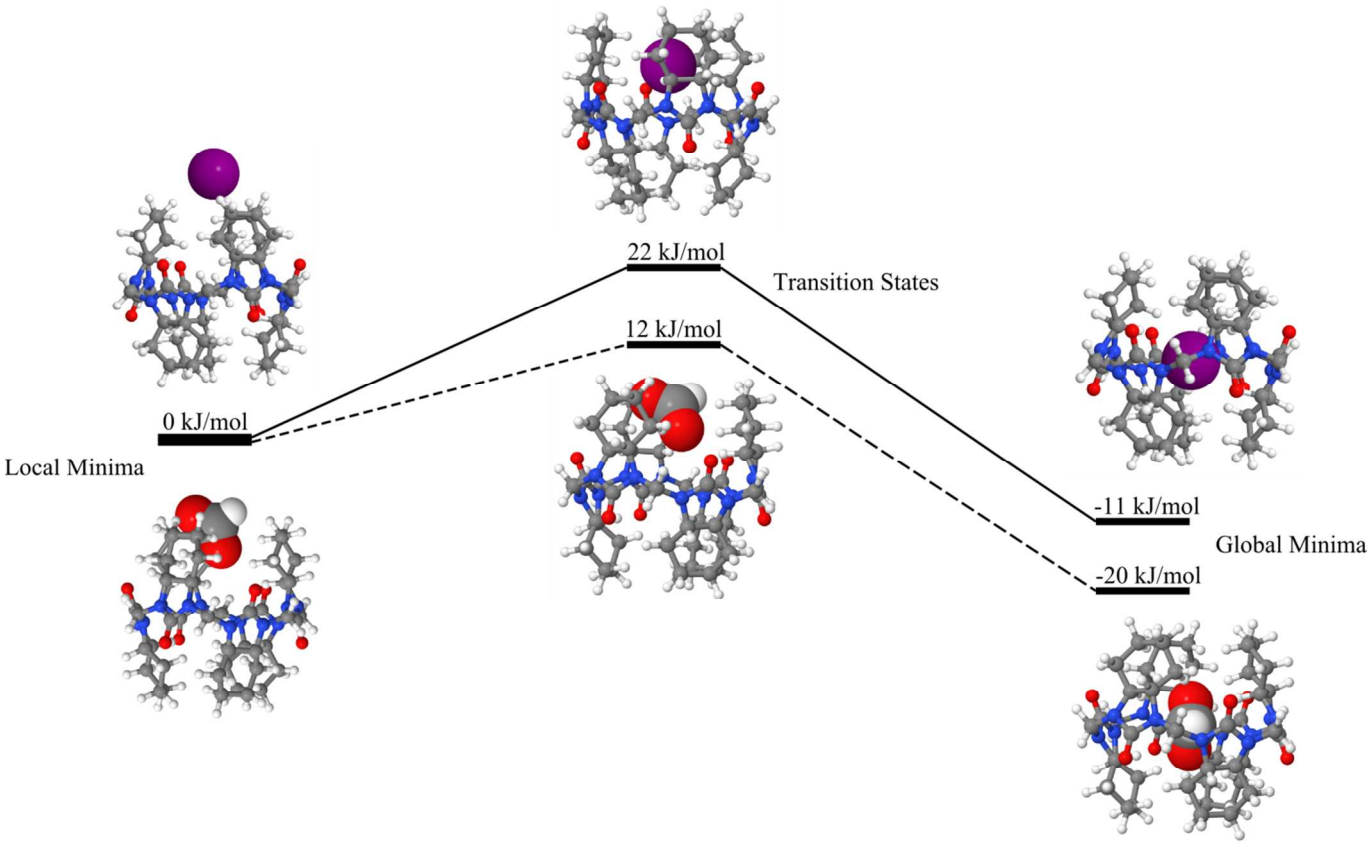

Fig.5. Reaction coordinates of I^- (solid line) and $HCOO^-$ (dashed line) forming inclusion complexes with cycHC[6].

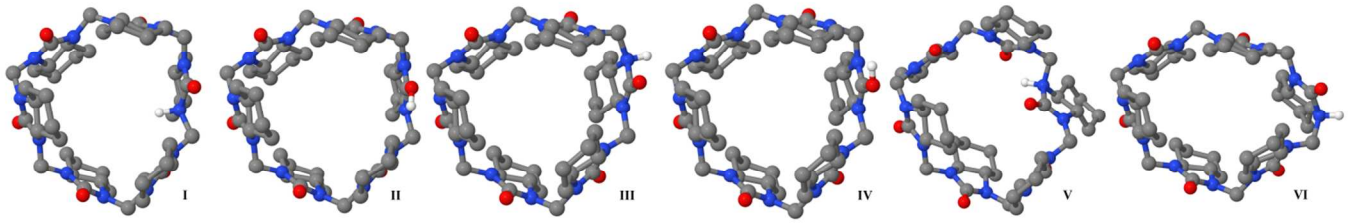

Fig.6. Structures of protonated cycHC[6]. Hydrogen atoms (except the added proton) were removed.

3.3 Structure of cycHC[6] with a proton.

The search for possible binding sites yielded six local minima for the proton. The lowest energy geometries with covalently bound protons are shown in Figure 6. Energetically, the binding of the proton to the macrocycle was favoured for all local minima, as shown in Table 4. The binding energy of the proton with the cycHC[6] was computed according to the reaction of cycHC[6] with oxonium as shown below:

$$H_3O^+ + \text{cycHC[6]} \rightarrow [\text{cycHC[6]} + H^+] + H_2O$$

Table 4. Energies (kJ/mol) of the protonation of cycHC[6]

Geometry nr	Protonation site of cycHC[6]	Energy difference from minima	Binding energy
I	at N_1 inside	0	-244
II	O	7	-238
III	at N_3 outside	9	-236
IV	O	11	-233
V	at N_3 inside	13	-232
VI	at N_1 outside	34	-211

The results show that, in reaction with an oxonium ion, cycHC[6] is preferably protonated at the nitrogen N_1 atom positioned inside of the macrocycle. According to the Boltzman distribution, the population of protonated geometry I will be over 90%. Favourable protonation sites were in good agreement with the analysis of the electronic structure of cycHC[6]. However, it should be noted that the binding of bulkier cations inside the cavity of the macrocycle is much less probable, due to the position and size of non-complexed cycHC[6] LUMO.

3.4 Structure of cycHC[6] with HCl, HBr, HI or HCOOH.

The non-dissociated guests can bind both inside and outside of the macrocycle. Energetically, the outside binding sites were favoured for all guests. The inclusion complexes were at least 14 kJ/mol higher in energy. The representative energetically favored geometries of the complex with hydrogen chloride are shown in Figure 7; the complexes with HBr, HI and HCOOH were similar. In contrast to the favourable binding site of the proton at the nitrogen of cycHC[6], there was binding of electron-poor hydrogens of non-dissociated acids at the oxygen atom of the macrocycle outside the cavity. This change in preferred interaction site is most probably caused by steric factors. The binding energies of these complexes confirm that complexation with non-dissociated acids was energetically favourable in the studied conditions (Table 5). The binding energies of the non-dissociated guests with cycHC[6] were computed according to the reaction shown below, where HX denotes the non-dissociated acid:

$$HX + \text{cycHC[6]} \rightarrow [\text{cycHC[6]} + HX]$$

Table 5. Binding energy (kJ/mol) of the non-dissociated guests with cycHC[6]

Non-dissociated Guest	Geometry	Energy difference from minima	Binding energy
HCl	a	0	-67
	b	2	-65
HBr	a	0	-26
	b	1	-25
HI	a	0	-31
	b	1	-30
HCOOH	a	5	-16
	b	0	-21

The results indicate that the cycHC[6] was able to bind the studied non-dissociated guests in the gas phase, although inclusion complexes were not formed.

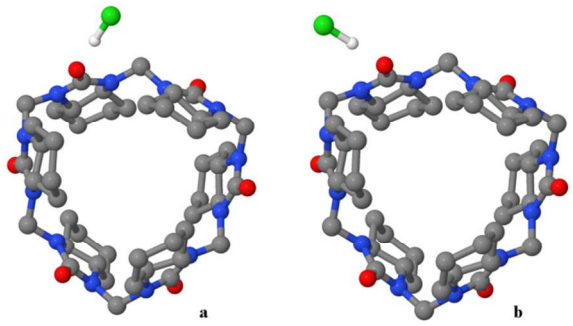

Fig.7. Lowest energy geometries of cycHC[6] and HCl complexes.

3.5 Ion-mobility mass-spectrometric analysis of cycHC[6] ion complexes

The computationally obtained structures were verified via TWIM-MS spectroscopy. The collision cross section (CCS) values measured by ion-mobility mass spectrometry and calculated from minimum energy conformers of Cl^-, Br^- and $HCOO^-$ anion complexes were found to agree with each other well (Table 6). The deviation of the calculated CCS from the experimental was 2%, confirming that anions formed inclusion complexes with cycHC[6]. The lowest-energy protonated cycHC[6] theoretical CCS value also coincided with the experimental data. It should be noted that the CCS of the $[\text{cycHC[6]}+Na]^+$ complex was significantly larger than all other ions' CCS, showing that sodium is positioned outside of the macrocycle.

Table 6. Collision cross section value of each trans-cycHC[6] complex.

Complex	Experimental CCS ($Å^2$)	Theoretical CCS ($Å^2$)
$[\text{cycHC[6]}+Cl]^-$	182	185
$[\text{cycHC[6]}+Br]^-$	183	186
$[\text{cycHC[6]}+HCOO]^-$	183	187
$[\text{cycHC[6]}+H]^+$	194	197 [a]
$[\text{cycHC[6]}+Na]^+$	225	-

[a] For geometry I in Fig.6 .

4. Conclusions

The electronic structure of *trans*-cyclohexylhemicucurbit[6]uril and its complexes with ionic (H^+, Cl^-, Br^-, I^- and $HCOO^-$) and non-dissociated (HCl, HBr, HI, HCOOH) guests was studied. It was shown that cyclohexylhemicucurbituril had numerous possible binding sites for all guests. The conclusions based on our study *in vacuo* are as follows:

(i) Non-complexed cyclohexylhemicucurbituril exhibited D_3 symmetry, and the computed geometry was in good agreement with the crystal structure. Calculations showed electron-rich areas on the oxygen atoms of each of the cyclohexylurea units, while the HOMO was located at the equator of the macrocycle.

The largest lobes of the HOMO were on nitrogen atoms, pointing inside and outside the macrocycle. Electron-deficient areas were located on methylene bridges and the centres of cyclohexyl groups. The LUMO was concentrated inside the macrocycle, filling the cavity.

(ii) All of the studied anions favoured binding inside the macrocycle. QTAIM analysis showed that twelve bonding interactions existed between the macrocycle and halogen anions, and fourteen such interactions were found between the macrocycle and $HCOO^-$. The order of the binding preference of the studied anions was $Cl^- > Br^- > HCOO^- > I^-$. The formation of the inclusion complex of anions with cycHC[6] was also confirmed by ion-mobility mass-spectrometry.

(iii) The systematic search for a binding site for a proton resulted in six possible locations. In the lowest-energy geometry, the proton was attached inside of the macrocycle to the nitrogen atom. Proton binding in the reaction of cycHC[6] with oxonium cation was favourable by -244 kJ/mol.

(iv) Non-dissociated acids preferred binding outside of the macrocycle through electron-poor hydrogens of the acids at the oxygen of cycHC[6]. There were two energetically close and structurally similar binding sites for all of the studied non-dissociated acids. According to the binding energy, -65 kJ/mol, the strongest complex was formed with hydrogen chloride.

Acknowledgements

This research was supported by the Estonian Science Foundation through Grant Nos. 8255 and 8698 and the Tallinn University of Technology basic financing grant No. B25. The Estonian Ministry of Education and Research through Grants IUT19-32 and the EU European Regional Development Fund (3.2.0101.08-0017) also provided financial support. Computations were performed on the HPC cluster at Tallinn University of Technology which is part of the ETAIS project. The authors thank Prof. Hugh I. Kim and Ms. Hyun Hee Lee L. Lee at the Pohang University of Science and Technology, Korea, for IM-MS data and helpful discussion. The authors would also like to thank Dr. Merle Uudsemaa at the Tallinn University of Technology for helpful discussion.

Notes and references

Department of Chemistry, Tallinn University of Technology, Ehitajate tee 5, 19086 Tallinn, Estonia

Electronic Supplementary Information (ESI) available: computational and IM-MS CCS details, including optimized geometries. See DOI: 10.1039/b000000x/

1. R. Behrend, E. Meyer and F. Rusche, *Justus Liebigs Ann. Chem.*, 1905, **339**, 1–37.
2. W. A. Freeman, W. L. Mock and N.-Y. Shih, *J. Am. Chem. Soc.*, 1981, **103**, 7367–7368.
3. E. Masson, X. Ling, R. Joseph, L. Kyeremeh-Mensah and X. Lu, *RSC Adv.*, 2012, **2**, 1213–1247.
4. B. C. Pemberton, R. Raghunathan, S. Volla and J. Sivaguru, *Chemistry*, 2012, **18**, 12178–12190.
5. S. Walker, R. Oun, F. J. McInnes and N. J. Wheate, *Isr. J. Chem.*, 2011, **51**, 616–624.
6. Y. Miyahara, K. Goto, M. Oka and T. Inazu, *Angew. Chem. Int. Ed. Engl.*, 2004, **43**, 5019–5022.
7. Y. Li, L. Li, Y. Zhu, X. Meng and A. Wu, *Cryst. Growth Des.*, 2009, **9**, 4255–4257.
8. T. Fiala and V. Sindelar, *Synlett*, 2013, **24**, 2443–2445.
9. M. Lisbjerg, B. M. Jessen, B. Rasmussen, B. Nielsen, A. Ø. Madsen and M. Pittelkow, *Chem. Sci.*, 2014, **5**, 2591–2908.
10. R. Aav, E. Shmatova, I. Reile, M. Borissova, F. Topić and K. Rissanen, *Org. Lett.*, 2013, **15**, 3786–3789.
11. H. Cong, T. Yamato, X. Feng and Zhu Tao, *J. Mol. Catal. A Chem.*, 2012, **365**, 181–185.
12. H. Cong, T. Yamato and Zhu Tao, *J. Mol. Catal. A Chem.*, 2013, **379**, 287–293.
13. H. Cong, T. Yamato and Zhu Tao, *New J. Chem.*, 2013, **37**, 3778–3783.
14. H.-J. Buschmann, E. Cleve and E. Schollmeyer, *Inorg. Chem. Commun.*, 2005, **8**, 125–127.
15. J. Svec, M. Necas and V. Sindelar, *Angew. Chem. Int. Ed. Engl.*, 2010, **49**, 2378–2381.
16. V. Havel, J. Svec, M. Wimmerova, M. Dusek, M. Pojarova and V. Sindelar, *Org. Lett.*, 2011, **13**, 4000–4003.
17. A. Révész, D. Schröder, J. Svec, M. Wimmerová and V. Sindelar, *J. Phys. Chem. A*, 2011, **115**, 11378–11386.
18. V. Havel, V. Sindelar, M. Necas and A. E. Kaifer, *Chem. Commun. (Camb).*, 2014, **50**, 1372–1374.
19. K. S. Oh, J. Yoon and K. S. Kim, *J. Phys. Chem. B*, 2001, **105**, 9726–9731.
20. H. Cong, Q.-J. Zhu, H.-B. Hou, S.-F. Xue and Zhu Tao, *Supramol. Chem.*, 2006, **18**, 523–528.
21. H. Cong, L.-L. Tao, Y.-H. Yu, Z. Tao, F. Yang, Y.-J. Zhao, S.-F. Xue, G. a Lawrance and G. Wei, *J. Phys. Chem. A*, 2007, **111**, 2715–2721.
22. F. Pichierri, *Dalton Trans.*, 2013, **42**, 6083–6091.
23. M. Sundararajan, R. V. Solomon, S. K. Ghosh and P. Venuvanalingam, *RSC Adv.*, 2011, **1**, 1333–1341.
24. M. Sundararajan, V. Sinha, T. Bandyopadhyay and S. K. Ghosh, *J. Phys. Chem. A*, 2012, **116**, 4388–4395.
25. S. Pan, S. Mondal and P. K. Chattaraj, *New J. Chem.*, 2013, **37**, 2492–2499.
26. R. V Pinjari and S. P. Gejji, 2008, **112**, 12679–12686.
27. R. V Pinjari and S. P. Gejji, *J. Phys. Chem. A*, 2009, **113**, 1368–1376.
28. P. H. Dixit, R. V Pinjari and S. P. Gejji, *J. Phys. Chem. A*, 2010, **114**, 10906–10916.
29. V. V Gobre, R. V Pinjari and S. P. Gejji, *J. Phys. Chem. A*, 2010, **114**, 4464–4470.
30. V. V. Gobre, P. H. Dixit, J. K. Khedkar and S. P. Gejji, *Comput. Theor. Chem.*, 2011, **976**, 76–82.
31. S. R. Peerannawar, V. V. Gobre and S. P. Gejji, *Comput. Theor. Chem.*, 2012, **983**, 16–24.
32. S. R. Peerannawar and S. P. Gejji, *J. Mol. Model.*, 2013, **19**, 5113–5127.

33. H. Cong, Y.-J. Zhao, S.-F. Xue, Zhu Tao and Q.-J. Zhu, *J. Mol. Model.*, 2007, **13**, 1221–1226.
34. J. W. Lee, S. Samal, N. Selvapalam, H.-J. Kim and K. Kim, *Acc. Chem. Res.*, 2003, **36**, 621–630.
35. T. S. Choi, J. Y. Ko, S. W. Heo, Y. H. Ko, K. Kim and H. I. Kim, *J. Am. Soc. Mass Spectrom.*, 2012, **23**, 1786–1793.
36. D. H. Noh, S. J. C. Lee, J. W. Lee and H. I. Kim, *J. Am. Soc. Mass Spectrom.*, 2014, **25**, 410–421.
37. H.-J. Buschmann and a. Zielesny, *Comput. Theor. Chem.*, 2013, **1022**, 14–22.
38. H.-J. Buschmann, A. Zielesny and E. Schollmeyer, *J. Incl. Phenom. Macrocycl. Chem.*, 2006, **54**, 181–185.
39. D.-D. Xiang, Q.-X. Geng, H. Cong, Zhu Tao and T. Yamato, *Supramol. Chem.*, 2014, 1–8.
40. N. Guex and M. C. Peitsch, *Electrophoresis*, 1997, **18**, 2714–2723.
41. M. D. Hanwell, D. E. Curtis, D. C. Lonie, T. Vandermeersch, E. Zurek and G. R. Hutchison, *J. Cheminform.*, 2012, **4**, 1–17.
42. P. A. M. Dirac, *Proc. R. Soc. A*, 1929, **123**, 714–733.
43. J. C. Slater, *Phys. Rev.*, 1951, **81**, 385–390.
44. S. H. Vosko, L. Wilk and M. Nusair, *Can. J. Phys.*, 1980, **58**, 1200–1211.
45. A. D. Becke, *Phys. Rev. A*, 1988, **38**, 3098–3100.
46. J. P. Perdew, *Phys. Rev. B*, 1986, **33**, 8822–8824.
47. F. Weigend and R. Ahlrichs, *Phys. Chem. Chem. Phys.*, 2005, **7**, 3297–3305.
48. P. Deglmann, K. May, F. Furche and R. Ahlrichs, *Chem. Phys. Lett.*, 2004, **384**, 103–107.
49. M. Sierka, A. Hogekamp and R. Ahlrichs, *J. Chem. Phys.*, 2003, **118**, 9136–9148.
50. K. Eichkorn, O. Treutler, H. Öhm, M. Häser and R. Ahlrichs, *Chem. Phys. Lett.*, 1995, **240**, 283–290.
51. K. Eichkorn, F. Weigend, O. Treutler and R. Ahlrichs, *Theor. Chem. Acc.*, 1997, **97**, 119–124.
52. K. A. Peterson, D. Figgen, E. Goll, H. Stoll and M. Dolg, 2003, **119**, 11113–11123.
53. K. A. Peterson, B. C. Shepler, D. Figgen and H. Stoll, *J. Phys. Chem. A*, 2006, **110**, 13877–13883.
54. P. Taylor, S. F. Boys and F. Bernardi, *Mol. Phys.*, 1970, **19**, 553–566.
55. O. Treutler and R. Ahlrichs, *J. Chem. Phys.*, 1995, **102**, 346–354.
56. M. Von Arnim and R. Ahlrichs, *J. Comput. Chem.*, 1998, **19**, 1746–1757.
57. R. Ahlrichs, M. Bär, M. Häser, H. Horn and C. Kölmel, *Chem. Phys. Lett.*, 1989, **162**, 165–169.
58. K. Eichkorn, F. Weigend, O. Treutler and R. Ahlrichs, *Theor. Chem. Acc.*, 1997, **97**, 119–124.
59. M. J. Frisch, G. W. Trucks, H. B. Schlegel, G. E. Scuseria, M. A. Robb, J. C. Cheeseman, J. R. Montgomery, Jr., J. A. Vreven, T. Kudin, K. N. Burant, J. M. Millam, S. S. Iyengar, J. Tomasi, V. Barone, B. Mennucci, M. Cossi, G. Scalmani, N. Rega, G. A. Petersson, H. Nakatsuji, M. Hada, M. Ehara, K. Toyota, R. Fukuda, J. Hasegawa, M. Ishida, T. Nakajima, Y. Honda, O. Kitao, H. Nakai, M. Klene, X. Li, J. E. Knox, H. P. Hratchian, J. B. Cross, V. Bakken, C. Adamo, J. Jaramillo, R. Gomperts, R. E. Stratmann, O. Yazyev, A. J. Austin, R. Cammi, C. Pomelli, J. W. Ochterski, P. Y. Ayala, K. Morokuma, G. A. Voth, P. Salvador, V. G. Dannenberg, J. J. Zakrzewski, S. Dapprich, A. D. Daniels, M. C. Strain, O. Farkas, D. K. Malick, J. B. Rabuck, A. D. Raghavachari, K. Foresman, J. V. Ortiz, Q. Cui, A. G. Baboul, S. Clifford, J. Cioslowski, B. B. Stefanov, G. Liu, A. Liashenko, P. Piskorz, I. Komaromi, R. L. Martin, D. J. Fox, T. Keith, M. A. Al-Laham, C. Y. Peng, M. Nanayakkara, A. Challacombe, P. M. W. Gill, B. Johnson, W. Chen, M. W. Wong, C. Gonzalez and J. A. Pople, *Gaussian 09, Revision C.01*, Gaussian, Inc., Wallingford CT, USA, 2004.
60. *Jmol: an open-source Java viewer for chemical structures in 3D*, http://www.jmol.org/ (accessed February 2014).
61. U. Varetto, Molekel version 5.4.0.8, Swiss National Supercomputing Centre, Lugano, Switzerland, 2006.
62. R. F. W. Bader, *Atoms in Molecules: A Quantum Theory*, Oxford University Press, Oxford, United Kingdom, 1990.
63. T. Lu, Multiwfn version 3.2.1, University of Science and Technology Beijing, Beijing, China, 2009.
64. E. Espinosa, E. Molins and C. Lecomte, *Chem. Phys. Lett.*, 1998, **285**, 170–173.
65. K. Thalassinos, M. Grabenauer, S. E. Slade, G. R. Hilton, M. T. Bowers and J. H. Scrivens, *Anal. Chem.*, 2009, **81**, 248–254.
66. www.indiana.edu/~clemmer, (accessed December 2013)
67. R. S. Rowland and R. Taylor, *J. Phys. Chem.*, 1996, **100**, 7384–7391.
68. T. Wyttenbach, G. Von Helden, J. J. Batka and M. T. Bowers, *J. Am. Soc. Mass Spectrom.*, 1997, **8**, 275–282.

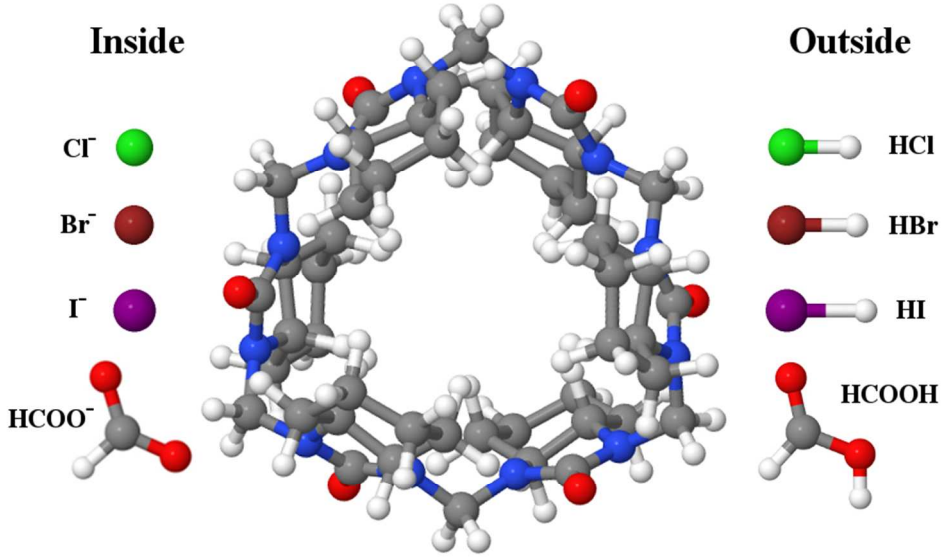

Binding properties of chiral cyclohexylhemicucurbit[6]uril and geometries of its complexes with anions, proton and non-dissociated acids.